Reactions of Gold Atoms and Small Clusters with CO: Infrared Spectroscopic and Theoretical Characterization of Au_nCO ($n = 1-5$) and $Au_n(CO)_2$ ($n = 1, 2$) in Solid Argon

Ling Jiang and Qiang Xu*

National Institute of Advanced Industrial Science and Technology (AIST), Ikeda, Osaka 563-8577, and Graduate School of Science and Technology, Kobe University, Nada Ku, Kobe, Hyogo 657-8501, Japan

Received: September 23, 2004; In Final Form: November 22, 2004

Laser-ablated Au atoms have been co-deposited with CO molecules in solid argon to produce gold carbonyls. In addition to the previously reported $Au(CO)_n$ ($n = 1, 2$) and $Au_2(CO)_2$ molecules, small gold cluster monocarbonyls Au_nCO ($n = 2-5$) are formed on sample annealing and characterized using infrared spectroscopy on the basis of the results of the isotopic substitution and CO concentration change and comparison with theoretical predictions. Of particular interest is that the mononuclear gold carbonyls, $Au(CO)_n$ ($n = 1, 2$), are favored under the experimental conditions of higher CO concentration and lower laser energy, whereas the yields of the gold cluster carbonyls, Au_nCO ($n = 2-5$) and $Au_2(CO)_2$, remarkably increase with lower CO concentration and higher laser power. Density functional theory (DFT) calculations have been performed on these molecules and the corresponding small naked gold clusters. The identities of these gold carbonyls Au_nCO ($n = 1-5$) and $Au_n(CO)_2$ ($n = 1, 2$) are confirmed by the good agreement between the experimental and calculated vibrational frequencies, relative absorption intensities, and isotopic shifts.

I. Introduction

The interaction of CO with transition-metal and main-group-element atoms, clusters, and surfaces plays a very important role in chemistry and chemical industry.[1,2] Many industrial processes employ CO as a reagent and transition-metal compounds as heterogeneous catalysts and involve the intermediates of metal carbonyls. As noble-metal compounds, gold carbonyls have been the subject of a number of studies. The first carbonyl derivative of gold, Au(CO)Cl, was reported in 1925.[3] Neutral gold mono- and dicarbonyls have been successfully synthesized in rare-gas matrixes by several groups.[4] Gold carbonyl cations, $[Au(CO)_n]^+$ ($n = 1, 2$), have been formed in superacid solutions or in the presence of weakly coordinating counteranions[5] and reported to be an excellent catalyst for carbonylation of olefins and alcohols.[6] Moreover, $[Au(CO)_n]^+$ ($n = 1-4$) have been generated and identified by the technique of laser ablation coupled with matrix isolation infrared spectroscopy.[4c]

Recently, it has been found that gold becomes catalytically active when deposited on select metal oxides as hemispherical ultrafine particles with diameters smaller than 5 nm.[7] The supported Au nanoparticles exhibit remarkable catalytic activities and/or excellent selectivities in a number of reactions such as low-temperature CO oxidation and reduction of nitrogen oxides.[7] In general, probe molecules (i.e., CO, H_2, H_2O, NO, NH_3, etc.) are used to gain insight into their chemisorption characteristics and catalytic activity. Reliable experimental data for neutral and charged clusters can be obtained, such as ionization potentials (IP), electron affinities (EA), magnetic moments, photoelectron spectra, infrared absorption spectra, polarizabilities, optical properties, and ligand adsorption capacities.[8] However, it is difficult to directly determine the structure of a metal cluster due to the fact that clusters are often produced in gas-phase beams and are too small (3−50 atoms) for applying diffraction techniques.[8] Fortunately, recent advances in methodology based on the technologies of pseudopotential and plane-wave basis sets and high-speed computers have now made it possible to obtain quantitative information on the cluster's structures as well as IP and EA, etc.[2,8]

The technique of laser ablation coupled with matrix isolation has proven to be an efficient method to generate neutral atoms and cations of transition metals[9] and main-group elements[10] as well as electrons. In addition to a large number of mononuclear metal carbonyls, small metal cluster carbonyls, such as Fe_2-CO,[11] Co_2CO,[12] B_2CO[13] and $B_2(CO)_2$,[14] M_nCO ($n = 2-5$; M = Si, Ge),[15] and Pb_nCO ($n = 1-4$),[16] have recently been synthesized via this combined approach. Meanwhile, theoretical investigations have been carried out for Fe_nCO ($n = 1-6$)[17] and Ni_2CO.[18] In contrast with considerable studies of mononuclear gold carbonyls,[3−6] however, much less is known about small gold cluster carbonyls. Here, we report the observation of the mono- and polynuclear gold carbonyls, Au_nCO ($n = 1-5$) and $Au_n(CO)_2$ ($n = 1, 2$), generated from reactions of gold atoms and small clusters with CO molecules in solid argon using infrared spectroscopy. Density functional theory (DFT) calculations have been performed to support the experimental assignments of the infrared spectra.

II. Experimental and Theoretical Methods

The experiment for laser ablation and matrix isolation infrared spectroscopy has been described previously[16,19] and is very similar to the technique reported earlier by Andrews' group.[9a] Briefly, the Nd:YAG laser fundamental (1064 nm, 10 Hz repetition rate with 10 ns pulse width) was focused on the rotating gold target. The laser-ablated gold atoms were co-deposited with CO in excess argon onto a CsI window cooled normally to 7 K by means of a closed-cycle helium refrigerator. Typically, 3−15 mJ/pulse laser power was used. Carbon monoxide (99.95% CO), $^{13}C^{16}O$ (99%, $^{18}O < 1\%$), and $^{12}C^{18}O$ (99%) were used to prepare the CO/Ar mixtures. In general, matrix samples were deposited for 1−2 h with a typical rate of

* To whom correspondence should be addressed. E-mail: q.xu@aist.go.jp.

10.1021/jp045681p CCC: $30.25
Published on Web 01/25/2005

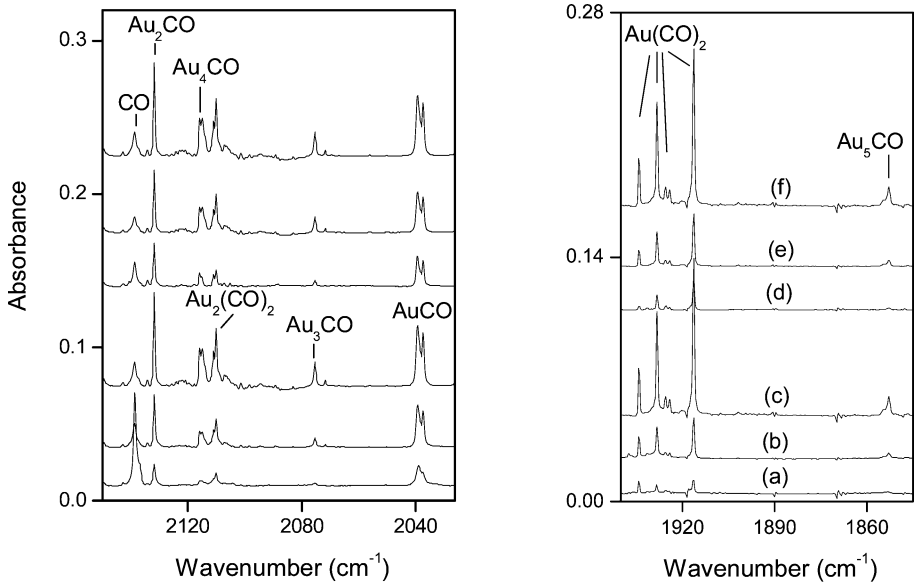

Figure 1. Infrared spectra in the 2160−1840 cm^{-1} region from co-deposition of laser-ablated Au atoms with 0.01% CO in Ar: (a) 1 h of sample deposition at 7 K, (b) after annealing to 30 K, (c) after annealing to 34 K, (d) after 15 min of broad-band irradiation, (e) after annealing to 38 K following d, and (f) 0.01% CO + 0.002% CCl_4 after annealing to 34 K.

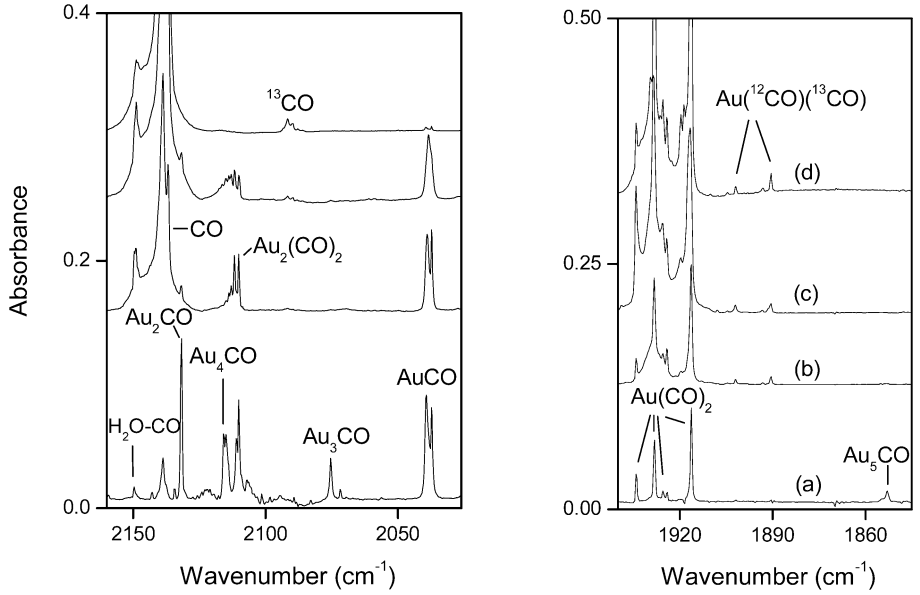

Figure 2. Infrared spectra in the 2160−1840 cm^{-1} region for laser-ablated Au atoms co-deposited with different CO concentrations in Ar after annealing to 34 K: (a) 0.01% CO, (b) 0.08% CO, (c) 0.2% CO, and (d) 0.4% CO.

2−4 mmol/h. After sample deposition, IR spectra were recorded on a BIO-RAD FTS-6000e spectrometer at 0.5 cm^{-1} resolution using a liquid nitrogen cooled HgCdTe (MCT) detector for the spectral range 5000−400 cm^{-1}. Samples were annealed at different temperatures and subjected to broad-band irradiation (λ > 250 nm) using a high-pressure mercury arc lamp (Ushio, 100 W).

Quantum chemical calculations were performed to predict the structures and vibrational frequencies of the observed reaction products using the GAUSSIAN 03 program.[20] The Becke three-parameter hybrid functional with the Lee−Yang−Parr correlation corrections (B3LYP) was used.[21] The 6-311+G-(d) basis sets were used for C and O atoms[22] and the Los Alamos ECP plus DZ for Au atoms.[23] Geometries were fully optimized and vibrational frequencies calculated with analytical second derivatives. Previous investigations have shown that the use of hybrid B3LYP along with ECP can provide reliable information for gold carbonyls, such as infrared frequencies, relative absorption intensities, and isotopic shifts.[4c]

III. Results and Discussion

Experiments have been done with carbon monoxide concentrations ranging from 0.01% to 0.4% in argon. Typical infrared spectra for the reactions of laser-ablated gold atoms with CO molecules in excess argon in the selected regions are shown in Figures 1−5, and the absorption bands in different isotopic experiments are listed in Table 1. The stepwise annealing and photolysis behavior of the product absorptions is also shown in the figures and will be discussed below. Experiments were also done with different concentrations of CCl_4 serving as an electron scavenger in solid argon. As can be seen in Figure 1, doping with CCl_4 has no effect on these bands, suggesting that the products are neutral.

Quantum chemical calculations have been carried out for all the possible isomers of the potential product molecules. Figure

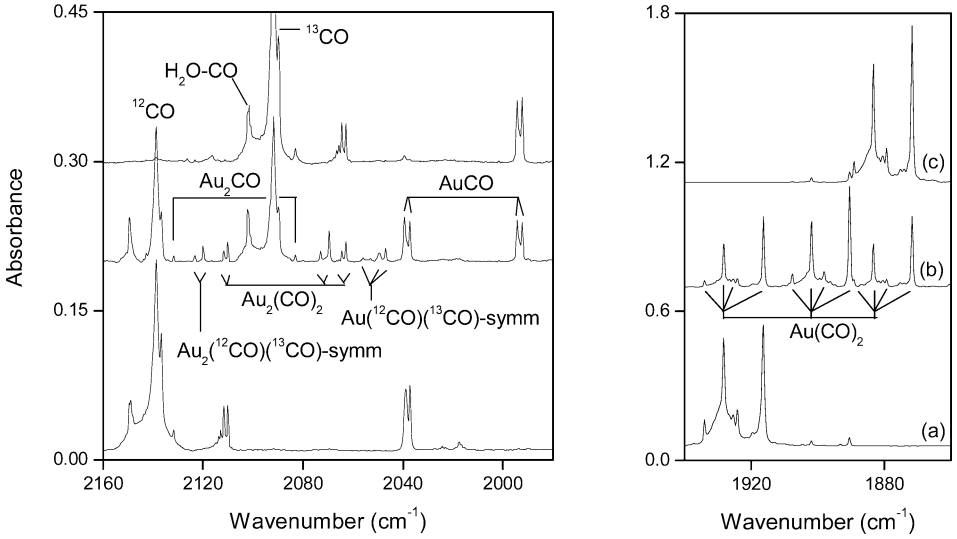

Figure 3. Infrared spectra in the 2160−1860 cm^{-1} region from co-deposition of laser-ablated Au atoms with isotopic CO in Ar after annealing to 34 K: (a) 0.08% $^{12}C^{16}O$, (b) 0.04% $^{12}C^{16}O$ + 0.04% $^{13}C^{16}O$, and (c) 0.08% $^{13}C^{16}O$.

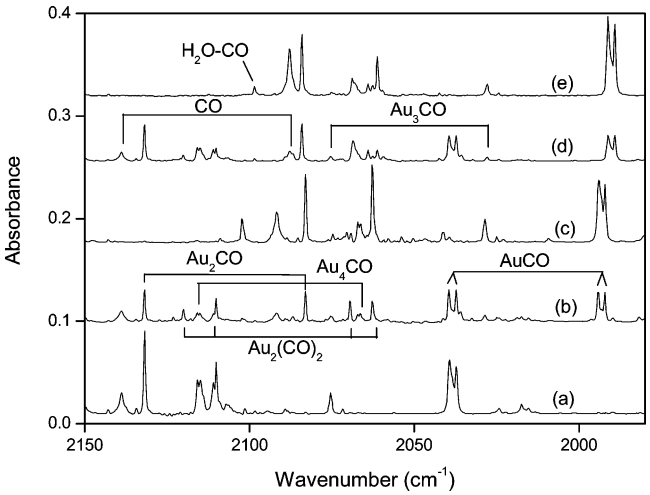

Figure 4. Infrared spectra in the 2160−1980 cm^{-1} region for laser-ablated Au atoms co-deposited with isotopic CO in Ar after annealing to 34 K: (a) 0.01% $^{12}C^{16}O$, (b) 0.005% $^{12}C^{16}O$ + 0.005% $^{13}C^{16}O$, (c) 0.01% $^{13}C^{16}O$, (d) 0.005% $^{12}C^{16}O$ + 0.005% $^{12}C^{18}O$, and (e) 0.01% $^{12}C^{18}O$.

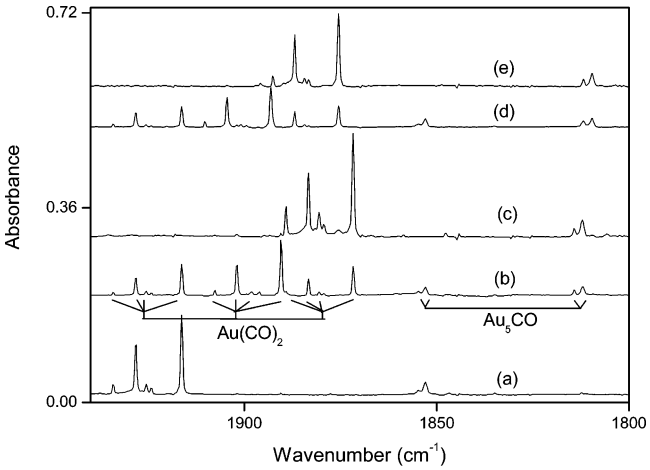

Figure 5. Infrared spectra in the 1940−1800 cm^{-1} region for laser-ablated Au atoms co-deposited with isotopic CO in Ar after annealing to 34 K: (a) 0.01% $^{12}C^{16}O$, (b) 0.005% $^{12}C^{16}O$ + 0.005% $^{13}C^{16}O$, (c) 0.01% $^{13}C^{16}O$, (d) 0.005% $^{12}C^{16}O$ + 0.005% $^{12}C^{18}O$, and (e) 0.01% $^{12}C^{18}O$.

6 shows the most stable structures of the reaction products. The ground electronic states, point groups, vibrational frequencies, and intensities are listed in Table 2. Table 3 reports a comparison of the observed and calculated isotopic frequency ratios for the C−O stretching modes of the reaction products.

A. AuCO and Au(CO)$_2$. The sharp band at 2039.3 cm^{-1} with a trapping site at 2037.2 cm^{-1} (Table 1 and Figures 1 and 2) has been observed on sample deposition. The main 2039.3 cm^{-1} band shifts to 1994.1 cm^{-1} with $^{13}C^{16}O$ and to 1991.3 cm^{-1} with $^{12}C^{18}O$. The mixed $^{12}C^{16}O$ + $^{13}C^{16}O$ and $^{12}C^{16}O$ + $^{12}C^{18}O$ isotopic spectra (Figures 3 and 4) only provide the sum of pure isotopic bands, indicating that only one CO subunit is involved in this mode. The isotopic $^{12}C^{16}O/^{13}C^{16}O$ and $^{12}C^{16}O/^{12}C^{18}O$ ratios are 1.0227 and 1.0241, respectively, also indicating single CO involvement. Accordingly, the 2039.3 cm^{-1} band is assigned to the C−O stretching mode of AuCO. The corresponding C−O stretching frequencies of AuCO in Ne, Kr, and Xe have been reported to be 2053.2, 2040.5, and 1985.5 cm^{-1}, respectively.[4a,c]

We also note that the 1916.3, 1925.4, 1928.2, and 1934.1 cm^{-1} bands increase together on sample annealing. Interestingly, the yields of these bands relative to the 2039.3 cm^{-1} band for AuCO sharply increase with higher CO concentration (i.e., 0.4%) and lower laser power (5 mJ/pulse) (Figure 2). As can be seen in Figure 3, four sets of triplet bands have been observed at 1916.3/1890.5/1871.7, 1925.4/1898.1/1879.4, 1928.2/1901.9/1883.3, and 1934.1/1907.7/1889.2 cm^{-1} in the mixed $^{12}C^{16}O$ + $^{13}C^{16}O$ isotopic spectra (Table 1). Similar isotopic spectra in the $^{12}C^{16}O$ + $^{12}C^{18}O$ experiments have also been obtained. These bands are assigned to the antisymmetric C−O stretching modes of the Au(CO)$_2$ molecule in different matrix sites, in agreement with previous studies.[4a,c] Weak bands have been observed for the symmetric CO stretching modes for Au(^{12}CO)(^{13}CO) and Au($C^{16}O$)($C^{18}O$) (Table 1).

Density functional theory (DFT) calculations lend strong support for the assignments. AuCO is predicted to have a bent geometry (Figure 6) with a $^2A'$ ground state (Table 2), which lies 4.51 kcal/mol lower than the linear structure. The CO binding energy in AuCO is 8.19 kcal/mol, which is in excellent agreement with the previous theoretical prediction (8.2 kcal/mol).[4c] The calculated C−O stretching frequency of the AuCO species is 2065.9 cm^{-1} (Table 2), which should be multiplied by 0.987 to fit the observed frequency. The calculated $^{12}C^{16}O/$

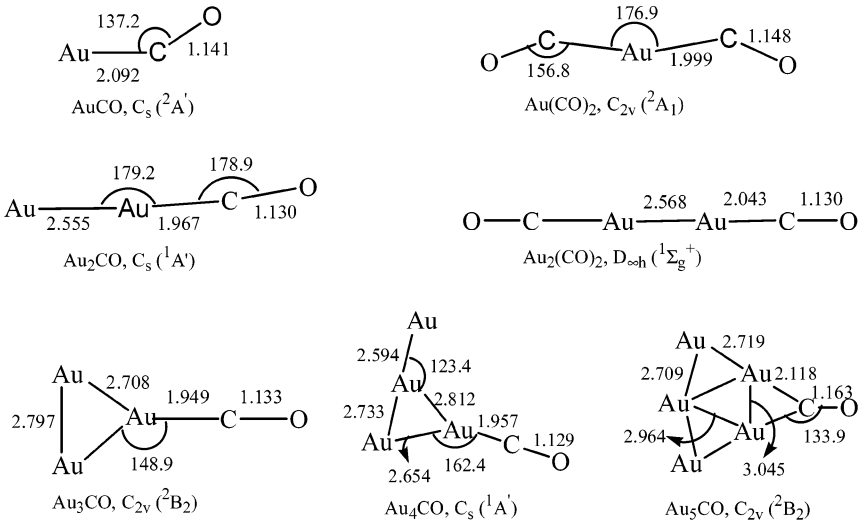

Figure 6. Optimized structures (bond lengths in Angstroms, bond angles in degrees) of the most stable isomers for the reaction products calculated at the B3LYP/6-311+G(d)-LANL2DZ level.

TABLE 1: Infrared Absorptions (cm^{-1}) Observed from the Reactions of Laser-Ablated Gold Atoms with CO in Excess Argon at 7 K

$^{12}C^{16}O$	$^{13}C^{16}O$	$^{12}C^{18}O$	$^{12}C^{16}O + {}^{13}C^{16}O$	$^{12}C^{16}O + {}^{12}C^{18}O$	*R*(12/13)	*R*(16/18)	assignment
2131.9	2083.0	2084.1	2131.9, 2083.1	2131.9, 2084.2	1.0235	1.0229	Au_2CO
2115.9	2067.2	2068.8	2115.9, 2067.2	2115.9, 2068.8	1.0236	1.0228	Au_4CO
2115.0	2066.4	2068.1	2115.0, 2066.4	2115.0, 2068.1	1.0235	1.0227	Au_4CO site
2111.0	2064.5	2064.1	2111.8, 2073.0, 2064.5, 2123.4 (sym)		1.0225	1.0227	$Au_2(CO)_2$ site
2110.2	2062.8	2061.2	2110.2, 2069.5, 2062.8, 2120.0 (sym)	2110.2, 2068.6, 2061.2, 2120.2 (sym)	1.0228	1.0237	$Au_2(CO)_2$
2075.4	2028.6	2027.9	2075.4, 2028.6	2075.4, 2028.0	1.0231	1.0234	Au_3CO
2039.3	1994.1	1991.3	2039.5, 1994.3	2039.4, 1991.2	1.0227	1.0241	AuCO
2037.2	1992.2	1989.1	2037.3, 1992.2	2037.3, 1989.1	1.0226	1.0241	AuCO site
1934.1	1889.1	1892.6	1934.1, 1907.7, 1889.2, 2056.0 (sym)	1934.1, 1910.2, 1892.6, 2071.9 (sym)	1.0238	1.0219	$Au(CO)_2$ site
1928.2	1883.3	1886.9	1928.2, 1901.9, 1883.3, 2051.8 (sym)	1928.2, 1904.5, 1886.9, 2062.7 (sym)	1.0238	1.0219	$Au(CO)_2$ site
1925.4	1879.4	1884.4	1925.4, 1898.1, 1879.4, 2049.6 (sym)	1925.4, 1900.9, 1884.4	1.0238	1.0218	$Au(CO)_2$ site
1916.3	1871.7	1875.5	1916.3, 1890.5, 1871.7, 2047.0 (sym)	1916.3, 1893.1, 1875.5, 2059.4 (sym)	1.0238	1.0218	$Au(CO)_2$
1854.8	1814.2	1811.8	1854.8, 1814.2	1854.8, 1811.8	1.0224	1.0237	Au_5CO site
1852.9	1812.1	1809.6	1852.9, 1812.0	1852.9, 1809.6	1.0225	1.0239	Au_5CO

TABLE 2: Ground Electronic States, Point Groups, Vibrational Frequencies (cm^{-1}), and Intensities (km/mol) of the Reaction Products Calculated at the B3LYP/6-311+G(d)-LANL2DZ Level

species	electronic state	point group	frequency (intensity, mode)
AuCO	$^2A'$	C_s	2065.9 (832, A′), 329.5 (5, A′), 210.7 (15, A′)
$Au(CO)_2$	$^2A_1$	C_{2v}	2103.4 (4, A_1), 1980.5 (3957, B_2), 389.1 (58, B_2), 377.0 (0.1, A_1), 296.5 (79, B_2), 257.6 (3, A_1), 257.6 (0, A_2), 132.7 (4, B_1), 53.0 (0.4, A_1)
$Au_2(CO)_2$	$^1\Sigma_g^+$	$D_{\infty h}$	2186.7 (0, σ_g), 2172.0 (1118, σ_u), 319.7 (0 × 2, π), 305.7 (0, σ_g), 260.6 (16 × 2, π), 258.9 (0, σ_u), 162.7 (0, σ_g), 26.0 (0 × 2, π), 21.1 (0 × 2, π)
Au_2CO	$^1A'$	C_s	2192.8 (588, A′), 368.4 (0.1, A′), 335.9 (9.0, A′), 282.5 (3, A″), 167.4 (4, A′), 47.5 (0, A′)
Au_3CO	$^2B_2$	C_{2v}	2169.2 (1226, A_1), 391.4 (6, A_1), 342.4 (5, B_1), 328.6 (1, B_2), 147.6 (3, A_1), 91.0 (0.3, A_1), 81.5 (2, B_2), 52.7 (0, B_1), 30.6(0.2, B_2)
Au_4CO	$^1A'$	C_s	2198.0 (819, A′), 380.6 (7, A′), 340.4 (1, A″), 335.8 (1, A′), 178.1 (5, A′), 139.7 (2, A′), 90.8 (2, A′), 75.8 (0.3, A′), 51.2 (0, A″), 36.0 (0, A′), 33.9 (0.1, A″), 19.6 (0.4, A′)
Au_5CO	$^2B_2$	C_{2v}	1923.7 (663, A_1), 376.1 (1, B_1), 369.5 (21, B_2), 296.6 (1, A_1), 188.9 (4, B_2), 157.0 (5, B_2), 131.2 (1, A_1), 95.8 (0, B_2), 93.8(0, A_1), 79.2 (0.3, A_1), 50.8 (0, A_1), 49.1 (0.2, B_2), 46.3 (0.3, B_1), 33.6 (0.2, B_1), 30.1 (0, A_2)

$^{13}C^{16}O$ and $^{12}C^{16}O/^{12}C^{18}O$ isotopic frequency ratios of 1.0225 and 1.0252 (Table 3) are consistent with the experimental values, 1.0227 and 1.0241, respectively. Similarly, the good agreement between the experimental and calculated vibrational frequencies, relative absorption intensities, and isotopic shifts confirms the identification of the $Au(CO)_2$ molecule. Briefly, $Au(CO)_2$ is predicted to have a $^2A_1$ ground state with C_{2v} symmetry and ∠CAuC = 176.9° (Table 2 and Figure 6), consistent with the previous report.[4c]

B. $Au_2(CO)_2$. The absorption at 2110.2 with a trapping site at 2111.0 cm^{-1} appears on sample deposition, observably increases on annealing, decreases on broad-band irradiation, and recovers on further annealing, as shown in Figure 1. The 2110.2 cm^{-1} band shifts to 2064.5 cm^{-1} with $^{13}C^{16}O$ and to 2061.2 cm^{-1} with $^{12}C^{18}O$ (Table 1, Figures 3 and 4). In the mixed

TABLE 3: Comparison of the Observed and Calculated Isotopic Frequency Ratios of the Reaction Products

		$^{12}C^{16}O/^{13}C^{16}O$		$^{12}C^{16}O/^{12}C^{18}O$	
molecule	mode	obsd	calcd	obsd	calcd
AuCO	C−O str.	1.0227	1.0225	1.0241	1.0252
$Au(CO)_2$	C−O asym-str.	1.0238	1.0235	1.0218	1.0238
$Au_2(CO)_2$	C−O asym-str.	1.0230	1.0230	1.0238	1.0244
Au_2CO	C−O str.	1.0235	1.0235	1.0229	1.0237
Au_3CO	C−O str.	1.0231	1.0236	1.0234	1.0235
Au_4CO	C−O str.	1.0236	1.0236	1.0228	1.0236
Au_5CO	C−O str.	1.0225	1.0228	1.0239	1.0247

$^{12}C^{16}O + {}^{13}C^{16}O$ experiment, a triplet at 2110.2, 2069.5, and 2062.8 cm^{-1} together with an associated band at 2120.0 cm^{-1} is observed. A similar isotopic splitting feature is obtained in the mixed $^{12}C^{16}O + {}^{12}C^{18}O$ isotopic spectra, indicating that two CO subunits are involved. As can be seen in Figure 2, the 2110.2 cm^{-1} band sharply increases with lower CO concentration (0.01%) and higher laser power (12 mJ/pulse) (Figure 2a), whereas the reverse is true for the relative yields of $Au(CO)_2$ bands. In the 0.01% CO and 12 mJ/pulse experiment the intensity ratio of the 2110.2, 2039.3, and 1916.4 cm^{-1} bands is 0.080:0.022:0.031, while this ratio changes to 0.019:0.052:0.550 in the 0.08% CO and 5 mJ/pulse experiment and to 0.009:0.139:0.280 in the 0.2% CO and 5 mJ/pulse experiment, suggesting that the molecule with the 2110.2 cm^{-1} band involves more Au atoms than AuCO and $Au(CO)_2$. This band is assigned to the antisymmetric C−O stretching mode of $Au_2(CO)_2$. The bands observed at 2120.0 cm^{-1} in the mixed $^{12}C^{16}O + {}^{13}C^{16}O$ experiment and 2120.2 cm^{-1} in the $^{12}C^{16}O + {}^{12}C^{18}O$ experiment are due to the symmetric C−O stretching modes of $Au_2(^{12}CO)(^{13}CO)$ and $Au_2(C^{16}O)(C^{18}O)$, respectively. The antisymmetric C−O stretching vibrations at 2110.2 and 2111.0 cm^{-1} are compatible with the previous neon matrix studies with 6.4 and 7.0 cm^{-1} blue shifts.[4c]

The assignment is strongly supported by the present DFT calculations, which predict this $Au_2(CO)_2$ molecule to have a linear geometry with a $^1\Sigma_g^+$ ground electronic state (Table 2 and Figure 6), in accord with the previous report,[4c] whereas nonlinear structures are observed for AuCO,[4c] $Au(CO)_2$,[4c] and Au_2CO (Figure 6). The antisymmetric C−O stretching frequency is calculated to be 2172.0 cm^{-1}, which requires a 0.972 scale factor. The calculated $^{12}C^{16}O/^{13}C^{16}O$ and $^{12}C^{16}O/^{12}C^{18}O$ isotopic frequency ratios of 1.0230 and 1.0244 (Table 3) are again in excellent agreement with the experimental values, 1.0230 and 1.0238, respectively.

C. Au_nCO ($n = 2-5$). The present infrared spectra provide evidence for the formation of small gold cluster carbonyls in the excess argon matrixes. For instance, weak bands at 2131.9, 2115.9, 2075.4, and 1852.9 cm^{-1} appear on sample deposition, which observably increase on sample annealing. The experimental conditions of lower CO concentration and higher laser power favors the formation of species with these bands (Figure 2). These bands have some trapping site absorptions (Table 1 and Figure 1), and we will focus on the main bands.

The 2131.9, 2115.9, 2075.4, and 1852.9 cm^{-1} absorptions shift to 2083.0, 2067.2, 2028.6, and 1812.1 cm^{-1} with $^{13}C^{16}O$ and to 2084.1, 2068.8, 2027.9, and 1809.6 cm^{-1} with $^{12}C^{18}O$, respectively. In the mixed $^{12}C^{16}O + {}^{13}C^{16}O$ and $^{12}C^{16}O + {}^{12}C^{18}O$ experiments, only pure isotopic counterparts are observed. The isotopic ratios ($^{12}C^{16}O/^{13}C^{16}O$:1.0235, 1.0236, 1.0231, and 1.0225; $^{12}C^{16}O/^{12}C^{18}O$: 1.0229, 1.0228, 1.0234, and 1.0239, respectively) and the mixed isotopic characteristic (Figures 4 and 5) indicate that only one CO subunit is involved in each mode. On the basis of their different isotopic frequency shifts and different annealing and photolysis behavior, each of these bands is attributed to one of the gold cluster carbonyls, Au_nCO with $n \geq 2$. The 2131.9, 2115.9, and 2075.4 cm^{-1} absorptions lie in the region expected for terminal-bonded C−O stretching vibrations, whereas the 1852.9 cm^{-1} band is due to a bridge-bonded C−O stretching vibration. The series experiments with different CO concentrations and laser energies show that the appearance of the 2131.9 cm^{-1} band is prior to the other three bands, which is assigned to the C−O stretching mode of Au_2CO. It is expected that a high Au/CO ratio favors the formation of higher clusters during annealing, as discussed in detail later (vide infra). The observed annealing behavior and the Au/CO ratio dependence, along with the DFT predictions, indicate that the bands at 2075.4, 2115.9, and 1852.9 cm^{-1} can be assigned to the C−O stretching vibrations of Au_3CO, Au_4CO, and Au_5CO, respectively.

It can be found from Tables 1−3 that the calculated frequencies (only 0.03%, 0.05%, 0.04%, and 0.04% higher, respectively) as well as the isotopic ratios are in excellent agreement with the experimental values. As shown in Figure 6, among the most stable gold cluster monocarbonyls, a terminal CO is found in Au_2CO, Au_3CO, or Au_4CO whereas a bridging CO in Au_5CO.

The present optimization results show that the naked Au_2 cluster has a $^1\Sigma_g^+$ ground state with the Au−Au bond of 2.574 Å, in accord with the experimental values (∼2.47 Å)[24] and the previous theoretical calculations (∼2.60 Å).[25] The Au−Au stretching of the Au_2 cluster is IR inactive, whereas the vibrational frequency of Au_2 was observed at 191 cm^{-1} in a study of emission and laser excitation spectra.[24] The most stable structure of the Au_2CO molecule is predicted to be asymmetric with a $^1A'$ ground state (Table 2 and Figure 6), which lies 27.77 kcal/mol lower than the bridge-bonded Au_2CO structure.

The naked Au_3 cluster has a $^2B_2$ ground state with C_{2v} symmetry, exhibiting an open obtuse angle structure with an apex angle of 64.8°, which is in accordance with the previous studies.[25a,b] Our DFT calculations predict that Au_3CO has a $^2B_2$ ground state with an Au−C bond of 1.949 Å. In Au_3CO, the apex angle (62.2°) is 2.6° smaller than that of Au_3 at the same DFT level. The bridge-bonded Au_3CO structure lies 23.31 kcal/mol higher than the most stable terminal-bonded one.

For Au_4, a planar rhombus arrangement with D_{2h} symmetry in the ^1A_g ground state is the most stable structure, in agreement with the previous studies.[25a,b] The most stable structure of Au_4CO is predicted to have a planar geometry with C_s symmetry, as shown in Figure 6. The CO molecule is terminal bonded to one of the apex Au atoms of the triangle Au_3 ring. The ∠CAuAu is calculated to be 162.4°. In the less stable Au_4CO, CO is terminal bonded to one of the apex Au atoms of a near rhombus Au_4. It is found that the Au_4CO with a near pyramid structure is 157.10 kcal/mol higher than the most stable one.

The naked Au_5 cluster is predicted to have a $^2A_1$ ground state with C_{2v} symmetry, in line with previous theoretical calculations.[25a,b] The most stable Au_5CO structure has a $^2B_2$ ground state with C_{2v} symmetry, and CO is bridge bonded to two Au atoms of Au_5 (Figure 6). In contrast, Si_5CO was predicted to have a nonplanar structure with C_{2v} symmetry in which CO bridges two of the equatorial silicon atoms of Si_5 with a trigonal bipyramid structure.[15a]

In addition, the calculated net charges of CO (not listed here) show that the partial electron is transferred from Au_n ($n = 1-5$) to CO, where Au_n behaves as a donor while CO behaves as an acceptor in bonding between Au_n and CO. Then, the C−O bond gains some activation as expected.

D. Reaction Mechanisms. With low CO concentrations and high laser energies the laser-ablated gold atoms react with CO molecules in the excess argon matrixes to produce the small gold cluster carbonyls, Au_nCO ($n = 2-5$) and $Au_2(CO)_2$, in addition to $Au(CO)_n$ ($n = 1, 2$) (Figure 1).

Under the present experimental conditions, gold atoms are the predominant species produced by laser ablation of the gold target. Only very small absorptions of the primary Au_nCO ($n = 2-5$) species are observed upon deposition, and these species appear and increase significantly upon sample annealing to high temperatures (30−34 K) in experiments with low CO concen-

TABLE 4: Energetics for Possible Reactions of Gold Atoms and Small Clusters with CO Calculated at the B3LYP/6-311+G(d)-LANL2DZ Level

no.	reaction	reaction energy[a] (kcal/mol)
1	$Au\ (^2S_{1/2}) + Au\ (^2S_{1/2}) \rightarrow Au_2\ (^1\Sigma_g^+)$	−43.20
2	$Au_2\ (^1\Sigma_g^+) + Au\ (^2S_{1/2}) \rightarrow Au_3\ (^2B_2)$	−20.27
3	$Au\ (^2S_{1/2}) + Au_3\ (^2B_2) \rightarrow Au_4\ (^1A_g)$	−44.04
4	$Au_2\ (^1\Sigma_g^+) + Au_2\ (^1\Sigma_g^+) \rightarrow Au_4\ (^1A_g)$	−21.11
5	$Au\ (^2S_{1/2}) + Au_4\ (^1A_g) \rightarrow Au_5\ (^2A_1)$	−40.22
6	$Au_2\ (^1\Sigma_g^+) + Au_3\ (^2B_2) \rightarrow Au_5\ (^2A_1)$	−41.06
7	$Au\ (^2S_{1/2}) + CO\ (^1\Sigma^+) \rightarrow AuCO\ (^2A')$	−8.19
8	$AuCO\ (^2A') + CO\ (^1\Sigma^+) \rightarrow Au(CO)_2\ (^2A_1)$	−13.04
9	$Au_2\ (^1\Sigma_g^+) + CO\ (^1\Sigma^+) \rightarrow Au_2CO\ (^1A')$	−25.56
10	$AuCO\ (^2A') + Au\ (^2S_{1/2}) \rightarrow Au_2CO\ (^1A')$	−60.56
11	$AuCO\ (^2A') + AuCO\ (^2A') \rightarrow Au_2(CO)_2\ (^1\Sigma_g^+)$	−65.09
12	$Au(CO)_2\ (^2A_1) + Au\ (^2S_{1/2}) \rightarrow Au_2(CO)_2\ (^1\Sigma_g^+)$	−60.25
13	$Au_2CO\ (^1A') + CO\ (^1\Sigma^+) \rightarrow Au_2(CO)_2\ (^1\Sigma_g^+)$	−12.72
14	$Au_3\ (^2B_2) + CO\ (^1\Sigma^+) \rightarrow Au_3CO\ (^2B_2)$	−26.27
15	$AuCO\ (^2A') + Au_2\ (^1\Sigma_g^+) \rightarrow Au_3CO\ (^2B_2)$	−38.35
16	$Au_2CO\ (^1A') + Au\ (^2S_{1/2}) \rightarrow Au_3CO\ (^2B_2)$	−20.99
17	$Au_4\ (^1A_g) + CO\ (^1\Sigma^+) \rightarrow Au_4CO\ (^1A')$	−29.40
18	$AuCO\ (^2A') + Au_3\ (^2B_2) \rightarrow Au_4CO\ (^1A')$	−65.25
19	$Au_2CO\ (^1A') + Au_2\ (^1\Sigma_g^+) \rightarrow Au_4CO\ (^1A')$	−24.96
20	$Au_3CO\ (^2B_2) + Au\ (^2S_{1/2}) \rightarrow Au_4CO\ (^1A')$	−47.17
21	$Au_5\ (^2A_1) + CO\ (^1\Sigma^+) \rightarrow Au_5CO\ (^2B_2)$	−13.65
22	$AuCO\ (^2A') + Au_4\ (^1A_g) \rightarrow Au_5CO\ (^2B_2)$	−45.67
23	$Au_2CO\ (^1A') + Au_3\ (^2B_2) \rightarrow Au_5CO\ (^2B_2)$	−29.15
24	$Au_3CO\ (^2B_2) + Au_2\ (^1\Sigma_g^+) \rightarrow Au_5CO\ (^2B_2)$	−28.43
25	$Au_4CO\ (^1A') + Au\ (^2S_{1/2}) \rightarrow Au_5CO\ (^2B_2)$	−24.46

[a] A negative value of energy denotes that the reaction is exothermic.

trations (see Figure 1), which indicates that these small gold clusters are mainly formed in solid argon upon annealing but not during the laser ablation process. This means that the higher laser power leads to neither generating more clusters in the gas phase nor significant annealing of the matrix during deposition and so increasing of the yield of Au_n species. It seems that a higher laser power accounts for the generation of a higher concentration Au in the matrix, corresponding to a higher Au/CO ratio.

The energetic analysis for possible reactions of gold atoms and small clusters with CO molecules has been performed at the B3LYP/6-311+G(d)-LANL2DZ level. As can be seen in Table 4, all the possible reactions of gold atoms and small clusters with CO are exothermic (−8.19 to −65.25 kcal/mol). This implies that the diffusion during annealing may make a species, i.e., a gold atom or cluster, a CO molecule, or a gold carbonyl intermediate, in the matrix readily react with its nearest neighbor, and consequently, the final product distribution will mainly depend on the Au/CO ratio, in agreement with our observations that low CO concentration and high laser power favor high nuclearity of cluster molecules (Figure 2). In contrast, at high CO concentration and low laser power, corresponding to a low Au/CO ratio, mononuclear gold polycarbonyl species are the predominant products.

IV. Conclusions

Reactions of laser-ablated Au atoms with CO molecules in solid argon have been studied using matrix-isolation infrared spectroscopy. In addition to the previously reported $Au(CO)_n$ ($n = 1, 2$) and $Au_2(CO)_2$ molecules, small gold cluster monocarbonyls Au_nCO ($n = 2-5$) are observed in the present infrared spectra. On the basis of the isotopic substitution, change of CO concentration, and comparison with density functional calculations, the absorptions at 2131.9, 2075.4, 2115.9, and 1852.9 cm^{-1} are assigned to Au_2CO, Au_3CO, Au_4CO, and Au_5CO, respectively. Among the most stable gold cluster monocarbonyls, a terminal CO is found in Au_2CO, Au_3CO, or Au_4CO whereas a bridging CO in Au_5CO. The experimental results of Au_nCO ($n = 1-5$) and $Au_n(CO)_2$ ($n = 1, 2$) are in good agreement with the prediction of density functional theory calculations.

Acknowledgment. The authors express sincere thanks to the referees for valuable comments and suggestions and gratefully acknowledge financial support for this research from AIST and Kobe University. L.J. thanks JASSO and Kobe University for an Honors Scholarship.

References and Notes

(1) Cotton, F. A.; Wilkinson, G.; Murillo, C. A.; Bochmann, M. *Advanced Inorganic Chemistry*, 6th ed.; Willy: New York, 1999. Ozin, G. A.; Mitchell, S. A. *Angew. Chem., Int. Ed. Engl*. **1983**, *22*, 674.

(2) Alonso, J. A. *Chem. Rev.* **2000**, *100*, 637.

(3) Manchot, W.; Gall, H. *Chem. Ber*. **1925**, *58*, 2175.

(4) (a) McIntosh, D.; Ozin, G. A. *Inorg. Chem*. **1977**, *16*, 51. (b) Kasai, P. H.; Jones, P. M. *J. Am. Chem. Soc*. **1985**, *107*, 6385. (c) Liang, B. Y.; Andrews, L. *J. Phys. Chem. A* **2000,** *104*, 9156.

(5) Willner, H.; Aubke, F. *Inorg. Chem*. **1990**, *29*, 2195. Willner, H.; Schaebs, J.; Hwang, G.; Mistry, F.; Jones, R.; Trotter, J.; Aubke, F. *J. Am. Chem. Soc*. **1992**, *114*, 8972.

(6) Xu, Q.; Imamura, Y.; Fujiwara, M.; Souma, Y. *J. Org. Chem*. **1997**, *62*, 1594. Xu, Q.; Souma, Y. *Top. Catal*. **1998**, *6*, 17. Xu, Q. *Coord. Chem. Rev*. **2002**, *231*, 83.

(7) Haruta, M.; Yamada, N.; Kobayashi, T.; Iijima, S. *J. Catal*. **1989**, *115*, 301. Haruta, M. *Catal. Today* **1997**, *36*, 153. Haruta, M. *Stud. Surf. Sci. Catal*. **2001**, *145*, 31. Sanchez-Castillo, M. A.; Couto, C.; Kim, W. B.; Dumesic, J. A. *Angew. Chem., Int. Ed. Engl*. **1983**, *43*, 1140. Sanchez, A.; Abbet, S.; Heiz, U.; Schneider, W. D.; Hakkinen, H.; Barnett, R. N.; Landman, U. *J. Phys. Chem. A* **1999**, *103*, 9573.

(8) Rösch, N.; Pacchioni, G. *Inorg. Chem*. **1990**, *29*, 2901. Rösch, N.; Ackermann, L.; Pacchioni, G. *J. Am. Chem. Soc*. **1992**, *114*, 3549. Rosen, A. *Adv. Quantum Chem*. **1998**, *30*, 235. Melomi, G.; Schmude, R. W.; Kingcade, J. E., Jr.; Gingerich, K. A., Jr. *J. Chem. Phys*. **2000**, *113*, 1852.

(9) (a) Burkholder; T. R.; Andrews, L. *J. Chem. Phys*. **1991**, *95*, 8697. (b) Zhou, M. F.; Andrews, L.; Bauschlicher, C. W., Jr. *Chem. Rev*. **2001**, *101*, 1931.

(10) Himmel, H. J.; Downs, A. J.; Greene, T. M. *Chem. Rev*. **2002**, *102*, 4191. Zhang, L. N.; Dong, J.; Zhou, M. F.; Qin, Q. Z. *J. Chem. Phys*. **2000**, *113*, 10169. Zhang, L. N.; Dong, J.; Zhou, M. F. *Chem. Phys. Lett*. **2001**, *334*, 335. Kong, Q. Y.; Chen, M. H.; Dong, J.; Li, Z. H.; Fan, K. N.; Zhou, M. F. *J. Phys. Chem. A* **2002**, *106*, 11709. Miao, L.; Shao, L. M.; Wang, W. N.; Fan, K. N.; Zhou, M. F. *J. Chem. Phys*. **2002**, *116*, 5643.

(11) Zhou, M. F.; Chertihin, G. V.; Andrews, L. *J. Chem. Phys*. **1998**, *109*, 10893. Zhou, M. F.; Andrews, L. *J. Chem. Phys*. **1999**, *110*, 10370. Tremblay, B.; Gutsev, G.; Manceron, L.; Andrews, L. *J. Phys. Chem. A* **2002**, *106*, 10525.

(12) Tremblay, B.; Manceron, L.; Gutsev, G.; Andrews, L.; Partridge, H., III *J. Chem. Phys*. **2002**, *117*, 8479.

(13) Zhou, M. F.; Wang, Z. X.; von Ragué Schleyer, P.; Xu, Q. *ChemPhysChem*. **2003**, *4*, 763.

(14) Zhou, M. F.; Tsumori, N.; Li, Z. H.; Fan, K. N.; Andrews, L.; Xu, Q. *J. Am. Chem. Soc*. **2002**, *124*, 12936.

(15) (a) Zhou, M. F.; Jiang, L.; Xu, Q. *J. Chem. Phys*. **2004**, *121*, 10474. (b) Zhou, M. F.; Jiang, L.; Xu, Q. *J. Phys. Chem. A*, submitted for publication.

(16) Jiang, L.; Xu, Q. *J. Chem. Phys*., in press.

(17) Gutsev, G. L.; Bauschlicher, C. W., Jr.; Andrews, L. *J. Chem. Phys*. **2003**, *119*, 3681.

(18) Ignatyev, I. S.; Schaefer, H. F., III; King, R. B.; Brown, S. T. *J. Am. Chem. Soc*. **2000**, *122*, 1989.

(19) Zhou, M. F.; Tsumori, N.; Andrews, L.; Xu, Q. *J. Phys. Chem. A* **2003**, *107*, 2458.

(20) Frisch, M. J.; Trucks, G. W.; Schlegel, H. B.; Scuseria, G. E.; Robb, M. A.; Cheeseman, J. R.; Montgomery, J. A., Jr.; Vreven, T.; Kudin, K. N.; Burant, J. C.; Millam, J. M.; Iyengar, S. S.; Tomasi, J.; Barone, V.; Mennucci, B.; Cossi, M.; Scalmani, G.; Rega, N.; Petersson, G. A.; Nakatsuji, H.; Hada, M.; Ehara, M.; Toyota, K.; Fukuda, R.; Hasegawa, J.; Ishida, M.; Nakajima, T.; Honda, Y.; Kitao, O.; Nakai, H.; Klene, M.; Li, X.; Knox, J. E.; Hratchian, H. P.; Cross, J. B.; Adamo, C.; Jaramillo, J.; Gomperts, R.; Stratmann, R. E.; Yazyev, O.; Austin, A. J.; Cammi, R.; Pomelli, C.; Ochterski, J. W.; Ayala, P. Y.; Morokuma, K.; Voth, G. A.; Salvador, P.; Dannenberg, J. J.; Zakrzewski, V. G.; Dapprich, S.; Daniels, A. D.; Strain, M. C.; Farkas, O.; Malick, D. K.; Rabuck, A. D.;

Raghavachari, K.; Foresman, J. B.; Ortiz, J. V.; Cui, Q.; Baboul, A. G.; Clifford, S.; Cioslowski, J.; Stefanov, B. B.; Liu, G.; Liashenko, A.; Piskorz, P.; Komaromi, I.; Martin, R. L.; Fox, D. J.; Keith, T.; Al-Laham, M. A.; Peng, C. Y.; Nanayakkara, A.; Challacombe, M.; Gill, P. M. W.; Johnson, B.; Chen, W.; Wong, M. W.; Gonzalez, C.; Pople, J. A. *Gaussian 03*, revision B.04; Gaussian, Inc.: Pittsburgh, PA, 2003.

(21) Lee, C.; Yang, E.; Parr, R. G. *Phys. Rev. B* **1988**, *37*, 785. Becke, A. D. *J. Chem. Phys*. **1993**, *98*, 5648.

(22) Krishnan, R.; Binkley, J. S.; Seeger, R.; Pople, J. A. *J. Chem. Phys*. **1980**, *72*, 650. McLean, A. D.; Chandler, G. S. *J. Chem. Phys*. **1980**, *72*, 5639.

(23) Wachter, J. H. *J. Chem. Phys*. **1970**, *52*, 1033. Hay, P. J. *J. Chem. Phys*. **1977**, *66*, 4377. Hay, P. J.; Wadt, W. R. *J. Chem. Phys*. **1985**, *82*, 299.

(24) Ames, L. L.; Barrow, R. F. *Trans. Faraday Soc*. **1967**, *63*, 39. Kordis, J.; Gingerich, K. A.; Seyse, R. J. *J. Chem. Phys*. **1974**, *61*, 5144 and references therein.

(25) (a) Häberlen, O. D.; Chung, S. C.; Rösch, N. *Int. J. Quantum Chem*. **1994**, *28*, 595. (b) Bravo-Pérez, G.; Garzón, I. L.; Novaro, O. *J. Mol. Struct. (THEOCHEM)* **1999**, *493*, 225. (c) Verga, S.; Fricke, B.; Nakamatsu, H.; Mukoyama, T.; Anton, J.; Geschke, D.; Heitmann, A.; Engel, E.; Bastuğ, T. *J. Chem. Phys*. **2000**, *112*, 3499.